TECHNICAL PROGRESS REPORT

A: COVER SHEET

Name of Submitting Organization: Nuonics, Inc.
Address of Submitting Organization: 1025 S. Semoran Blvd, Suite 1093, Winter Park, FL 32792
Tel/Fax: 407-379-0164

Name & Address of Sub-Contractors: (a) University of Central Florida, 4000 Central Florida Blvd., CREOL Bldg, Orlando, FL 32816-2700 and (b) AppliCote Associates, LLC, 3259 Progress Drive A, Orlando, FL 32826.

DOE Award No.: DE-FC26-03NT41923

Project Title: Ultra-High Temperature Sensors Based on Optical Property Modulation and Vibration-Tolerant Interferometry

Dated: Jan. 26, 2006.

Principal Author: Dr. Nabeel A. Riza (email: nriza@aol.com)

Period Covered by Report: July 1, 2005 – Dec. 31, 2005.
Type of Report: Semi-Annual Technical Progress Report

B: ABSTRACT

The goals of the second six months of the Phase 2 of this project were to conduct first time experimental studies using optical designs and some initial hardware developed in the first 6 months of Phase 2. One focus is to modify the SiC chip optical properties to enable gas species sensing with a specific gas species under high temperature and pressure. The goal was to acquire sensing test data using two example inert and safe gases and show gas discrimination abilities. A high pressure gas mixing chamber was to be designed and assembled to achieve the mentioned gas sensing needs. Another goal was to initiate high temperature probe design by developing and testing a probe design that leads to accurately measuring the thickness of the deployed SiC sensor chip to enable accurate overall sensor system design. The third goal of this phase of the project was to test the SiC chip under high pressure conditions using the earlier designed calibration cell to enable it to act as a pressure sensor when doing gas detection. In this case, experiments using a controlled pressure system were to deliver repeatable pressure measurement data. All these goals have been achieved and are described in detail in the report. Both design process and diagrams for the mechanical elements as well as the optical systems are provided. Photographs or schematics of the fabricated hardware are provided. Experimental data from the three optical sensor systems (i.e., Thickness, pressure, and gas species) is provided. The design and experimentation results are summarized to give positive conclusions on the proposed novel high temperature high pressure gas species detection optical sensor technology.

C: TABLE OF CONTENTS

D: LIST OF GRAPHICAL MATERIALS

Fig.13 SiC Optical Chip top surface profile measured using a white light interferometer.

Fig.14 A cross-section taken through Figure 13 showing the characteristic surface flatness of the chip.

Fig.15 shows the distribution histogram of the SiC chip surface profile image.

Fig.16. The surface profile taken at another location on the SiC chip and its corresponding cross-section is shown in Fig.17.

Fig.17. The surface profile cross-section taken from the Fig.16 chip image.

Fig.18. Proposed SiC-chip based wireless optical pressure sensor system.

Fig.19 Experimental laboratory set-up for the SiC chip-based pressure sensor system.

Fig.20. Close-up view of the experimental SiC chip mounted in the high pressure cell.

Fig.21. SiC chip-based pressure system $I_i(x,y)$ optical images produced for (a) 1 atm, (b) 13.6 atm (200 psi), (c) 27.2 atm (400 psi), and (d) 40.8 atm (600 psi) high pressure conditions.

Fig.22. Optical pressure system response versus applied pressure for the SiC chip under test.

Fig. 23: Mechanical Models of SiC Sensor Chip, (a) Clamped Edge model and (b) Simply Supported model.

Fig. 24: The expected **(a)** deflection and **(b)** stress produced in 6H Silicon Carbide sensor chip of 5mm pressure seal diameter and 280 μm thickness.

Table 1: Experimental Results for the Calculated Thickness for SiC and Si.

E: INTRODUCTION

The purpose of this project is to develop a science base to fabricate sensors for ultra high temperature fossil fuel applications. The sensors proposed are based on the principle of the Optical Path Length (OPL) variation in a medium owing to the dependence of the optical property (e.g., refractive index) of a high temperature material, such as silicon carbide (SiC), on the temperature, pressure, or species concentration. These three thermodynamic variables can be measured by a single sensor if we understand how they individually change the refractive index of the sensor material. Since these changes can be very small, a high accuracy optical signal processing scheme is proposed for working in unison with the remote SiC sensor frontend. Specifically, a vibration-tolerant interferometric technique capable of measuring the changes in OPL with sub-nanoscale accuracy and at a high speed is investigated in this project. The proposed novel sensor technique will thus enable us to measure the desired variables remotely, accurately and rapidly.

Remote interrogation of the sensor by using a laser beam will eliminate the complications associated with electrical signal-based sensors in high temperature applications. The complications in such conventional sensors include (i) melting of the solder joint between the sensor device and the bonding wire, (ii) requirement of high temperature insulation for the electrical wires connecting the device to the electrical signal processing unit, and (iii) inconvenience in mounting or embedding the device in rotating components such as the turbine blades. A high speed optical interferometer can respond to the changes in the thermodynamic variables rapidly at microsecond speeds allowing real-time control of the combustion process.

Since a passive sensor frontend chip is proposed, any optically transparent high temperature material, such as a single crystal silicon carbide, diamond or sapphire, can be used as the sensor

chip material. Such a passive sensor chip can be custom fabricated for specific gas species detection and produced at low cost in a small (sub-millimeter) size and can be readily embedded in a small hole at the surface of any structure by using the thermal expansion/contraction stress-based fitting method. The structure could be a stationary or rotating component containing the sensor at a convenient location providing remote accessibility to the probe laser beam for interferometry.

Note that the leading fiber-optic sensors such as using fiber Fabry-Perot interference or in-fiber Bragg Gratings with wavelength-based processing require costly environmental protection of the light delivery and light return fiber [1-3]. This is because the fiber intrinsically contains both the sensing zone that must react to the changing environmental conditions (e.g., temperature) and the light delivery fiber that should stay protected and essentially unaffected from changing environmental effects (e.g., changing stresses in the long lengths of the delivery fiber could cause unexpectedly high bending losses leading to loss of detection signal). It is well known that standard low loss single mode optical fibers (SMFs) are made of glass, with transition temperatures around 475 °C, leading to unwanted softening of glass at higher temperatures, such as needed in DOE applications. Thus, there exists a dilemma for the sensor design engineer using the mentioned fiber-optic sensors. In our proposed sensor, this dilemma is removed as a free-space laser beam reads sensing parameters off the SiC sensor chip, thus producing no physical contact between the harsh environment and the light delivery and processing optics. In effect, one can imagine many low cost SiC optical chips distributed in the desired sensing zone where a scanning free-space laser beam rapidly engages these sensor frontend chips to produce signals for later data processing and environmental parameter recovery. In effect, a truly non-invasive distributed optical sensor is realized.

F: EXECUTIVE SUMMARY

Accomplishments during the first six months of this project have been achieved on three fronts, namely; SiC chip processing and gas species detection under high temperature and pressure, super accurate SiC chip thickness measurement for proper temperature probe and sensor design, and SiC optical chip mechanical performance and measurement under high pressure.

The first objective was achieved by initially studying the optical response of a SiC chip that was metallized by laser processing to change its optical properties within the crystal structure. A high power laser beam was used to implement this material change process. Second, a gas species optical sensor system configuration was setup by complementing the high temperature high pressure assembly originally designed and used in the first phase of the project. This new setup involves a new high pressure gas mixing system that allows the controlled introduction of independent gas species into the SiC chip-based optical assembly that is also subjected to high temperatures and pressures. Data gathered using this system indicates specific optical power responses to two different gas species and to different temperatures and pressures.

The second objective was achieved by designing the proposed optical temperature probe sensor system as a SiC chip thickness measurement system. Here a hybrid fiber-freespace design is shown to be a self-calibrating true thickness measurement system for the SiC chip. The approach uses selective wavelength interferometry in combination with prior known SiC Sellmeier material dispersion equation to provide a highly accurate sensor chip thickness reading. Experimental data indeed shows sub-micron precision thickness readings allowing accurate design of the proposed SiC chip-based optical probe and wireless sensor systems.

The third objective was achieved by incorporating the earlier phase assembled calibration test cell with a pressure sealed SiC chip to study effects of high gas pressure on the chip and its mechanical and optical response. Experimental results show that proper choice of the SiC chip pressure seal boundary conditions enables small scale chip mechanical deformations that indeed are amplified by optical readout and monitoring of the global optical spatial interference pattern. Data indicates that the SiC chip is robust for high pressure measurement as required for the design of the proposed gas species sensor.

G: EXPERIMENTAL RESULTS

G.1 Fabrication and Testing of SiC Chip for High Temperature High Pressure Gas Species Detection:

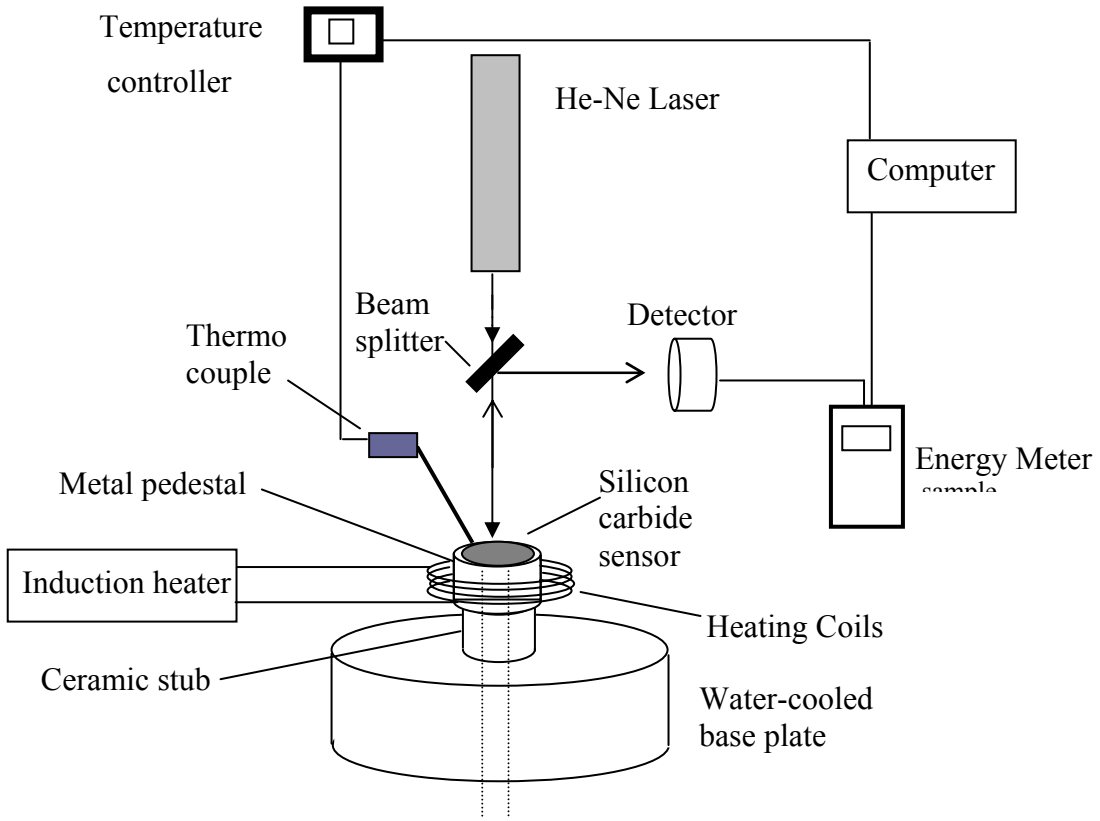

Figure 1. The original experimental hardware design used for high temperature optical characterization of various SiC chip samples.

The optical properties of two different 6H-SiC samples (A & B) obtained from different batches of SiC crystal growth process are investigated using the Fig.1 set-up engaging a 632.8 nm He-Ne Laser. These were single crystal wafers of typical diameter 2.54 cm. The thicknesses of samples A and B were measured to be 380 μm and 420 μm respectively. The samples were cleaned chemically before conducting reflected power measurement experiments. The polished SiC chip sample is placed on a stainless steel pedestal of diameter 2.9 cm. A water-cooled copper coil

connected to a water-cooled induction heater is used to heat the pedestal. The pedestal is placed at the center of the coil to achieve uniform heating of the pedestal. The heat from the pedestal raises the temperature of the chip, as used in our earlier Phase I (year 1) experiments. The pedestal also contains a small hole of 7.9 mm diameter that provides the open/active chip area for the reflected optical power measurements. The volume beneath this chip area represents the gas species control volume to which the chip will be in contact with in gas detection under high pressure applications. The temperature of the chip is measured with a thermocouple connected to a temperature controller. Data collection process was time synchronized and computerized to provide accurate value of the themo-couple temperature reading and chip reflected optical power. The optical power from the chip is studied for both normal incident angle (0º) and oblique incident angle (45º) of the He-Ne laser beam. For normal incidence, the beam is partially transmitted through a beam splitter placed at 45° angle with respect to the incident beam. The Beam Splitter (BS) was specifically designed to operate at 632.8 nm wavelength. For oblique incidence, the reflected power was measured without the beam splitter. To understand the difference in the optical response of samples A and B, their dopant concentrations were analyzed using SIMS. The dopant concentration affects the refractive index and consequently, the reflectivity of the chip. As shown in Figs. 2(a) and 2(b), several sets of the optical power versus temperature for 1 bar pressure conditions were measured for the SiC chip samples A and B. This data has the expected oscillatory patterns as shown in our earlier Phase I work.

Note that the amplitude of the oscillatory pattern is less for sample A than for sample B, a result partly due to the different sample fabrication conditions where the type and amount of dopant atoms affect the optical response of the SiC wafer. The dopant concentrations in SiC samples A and B from earlier works are shown in Figs. 3 and 4, respectively.

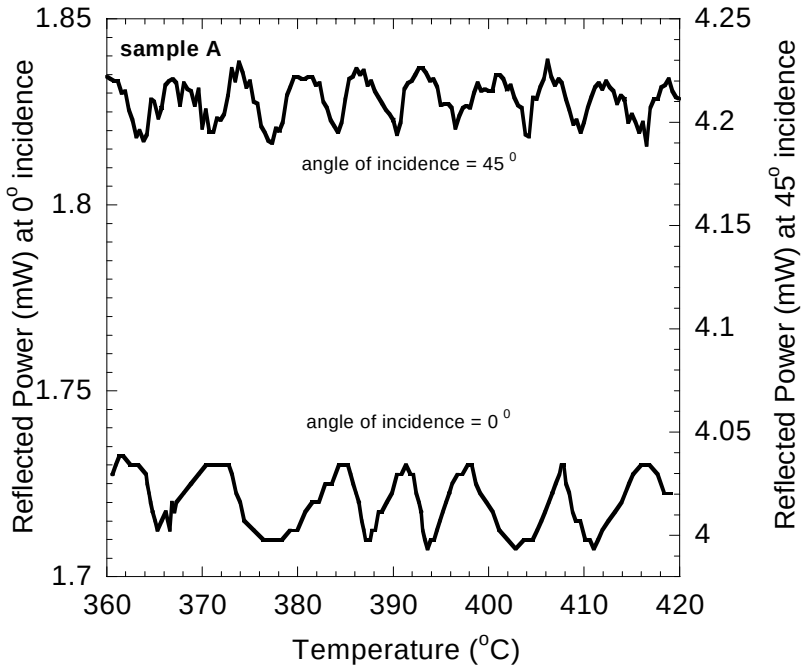

Figure 2a. Optical power for SiC doped sample A as a function of temperature from 27°C up-to 750°C for 0° and 45° incidence angle.

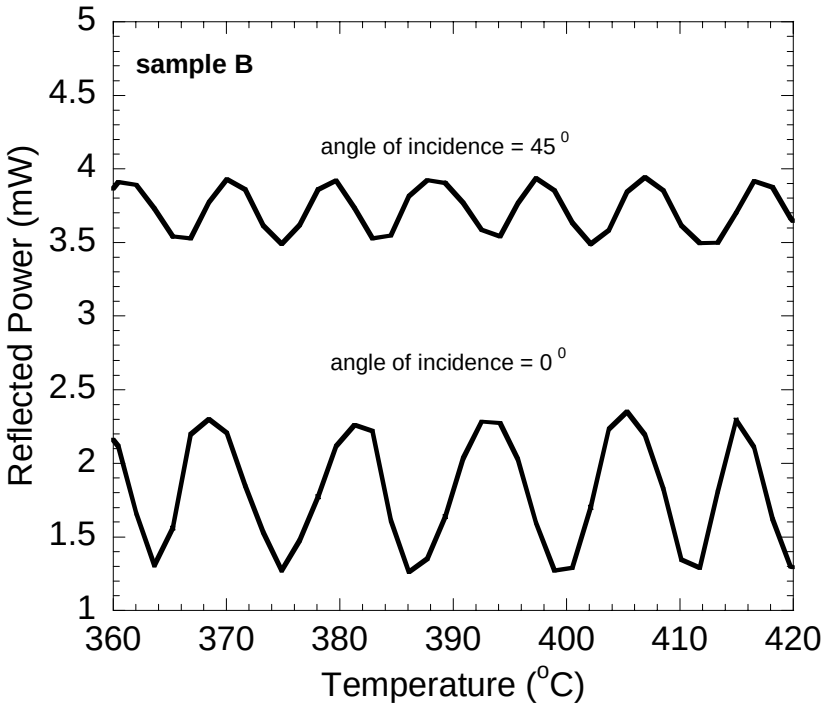

Figure 2b. Reflected power for sample B as a function of temperature from 27°C up to 750°C for 0° and 45° incidence angle.

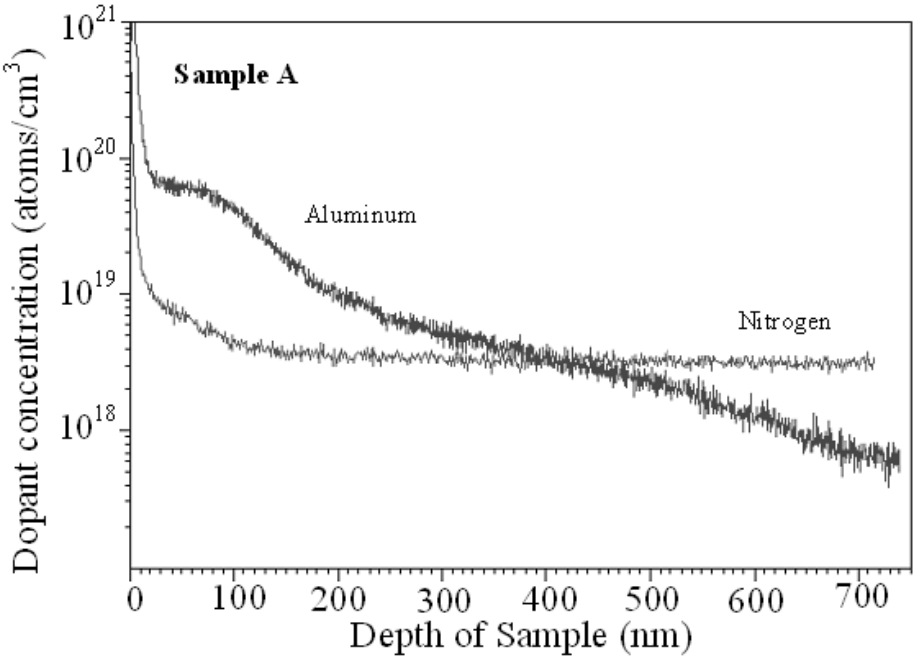

Figure 3. Concentration depth profiles of Aluminum and Nitrogen measured with SIMS for sample A of thickness 380 μm.

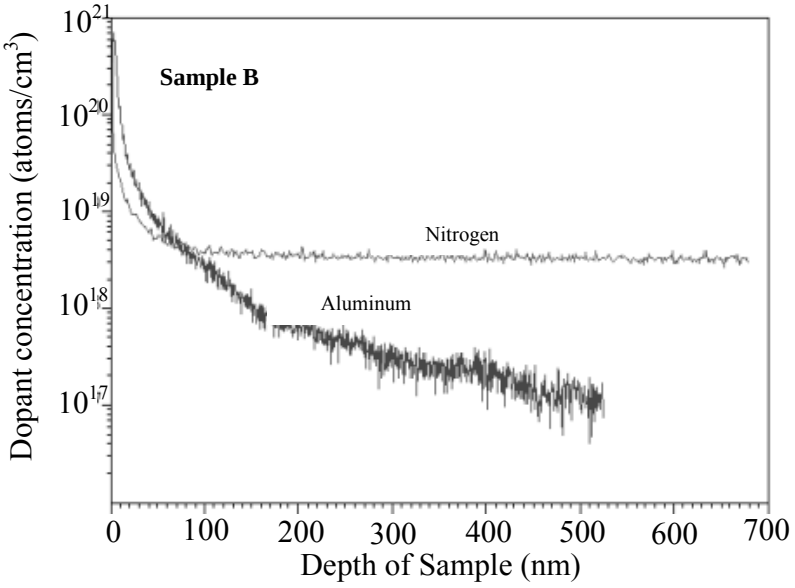

Figure 4. Concentration depth profiles of Aluminum and Nitrogen measured with SIMS for SiC sample B of thickness 420 μm.

Next, a laser metallized SiC chip sample A was produced by a process is known as laser metallization [4] and [5] in which localized heating by the high intensity laser beam disorders the

crystalline structure of SiC and produces carbon-rich phases which usually exhibit metal-like properties.

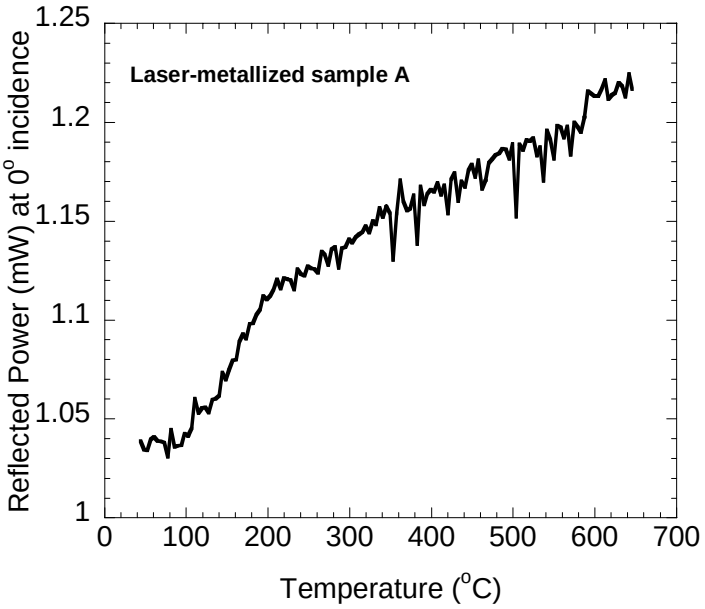

Figure 5.Optical power vs. temperature for the laser-metallized SiC sample A for a normal incidence 6.7 mW He-Ne laser beam (LAMMP Lab Data).

The laser parameters were chosen properly to modify the microstructure inside sample A using a high intensity Nd:YAG pulsed laser beam with an average laser power = 2.5 W, a pulse repetition rate = 5 kHz, a focused beam radius at the surface of the sample of 55 μm, a laser beam diameter of 5 mm above the top surface of the sample, and a writing laser beam scanning speed = 1 mm/s in the presence of an Argon gas at a 30 psi pressure. Fig.5 shows some basic and initial optical power measurements from this metalized SiC chip, indicting a monotonic function of power versus temperature. Because the metallized optical phase layer is embedded within the chip, the chip optical properties are expected to stay robust due to harsh environmental effects such as found in fossil-fuel based power generation systems. Hence, this embedded sensor chip structure offers new promise for sensor systems such as gas specific sensor chips.

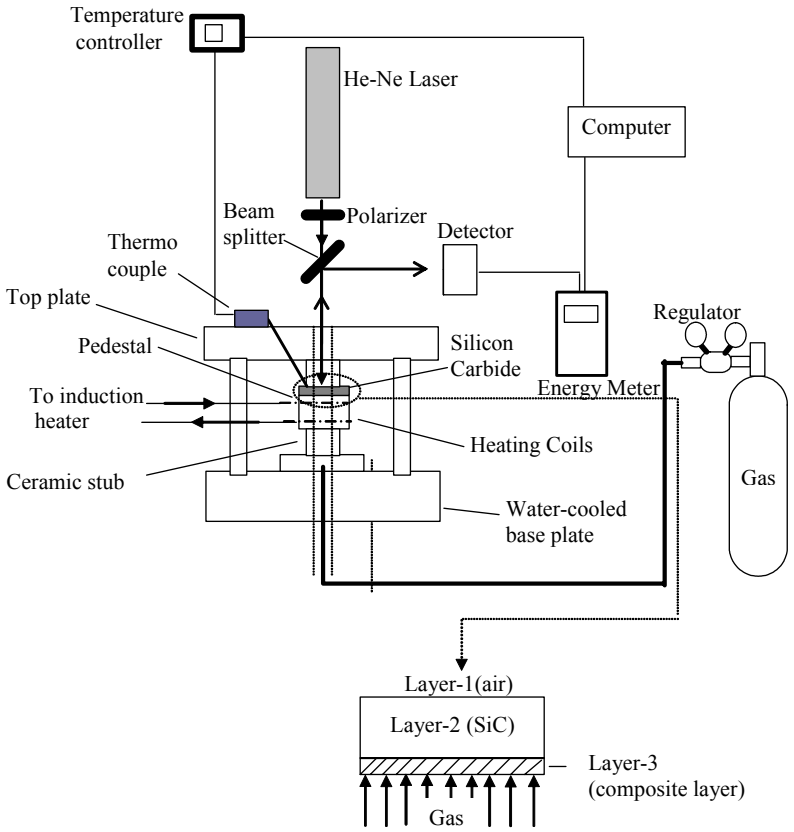

Figure 6. Schematic layout of the experimental setup used for studying SiC optical response due to different gas pressure and two different but independently used gas types.

SiC chip Sample B was used as a chip element in the Fig. 6 gas test system. As mentioned, the pedestal contains a small hole of 7.9 mm diameter that creates a 50 mm^2 area for the reflected power interrogation measurement. The volume of the hole beneath this chip area is filled with different gases through a gas feed mechanism and the pressure of the gas is controlled with a high-pressure regulator. To hold the chip in place against this gas pressure, a ceramic insulator is placed on top of the chip and then a copper plate is mounted on the ceramic insulator. The copper plate is secured to three copper posts attached to a stainless steel base plate. The copper plate and the ceramic insulator have a hole at the center similar to the pedestal to interrogate the chip. The continuous wave He-Ne laser is used to test the SiC chip optical power response as a

function of temperature, gas-type, and gas pressure with data obtained at high temperatures (up to 300°C) and pressures (up to 400 psi).

At varying pressures, Figures 7 and 8 represent the measured optical power from the sample B SiC chip when its bottom surface is exposed to nitrogen and argon gases, respectively.

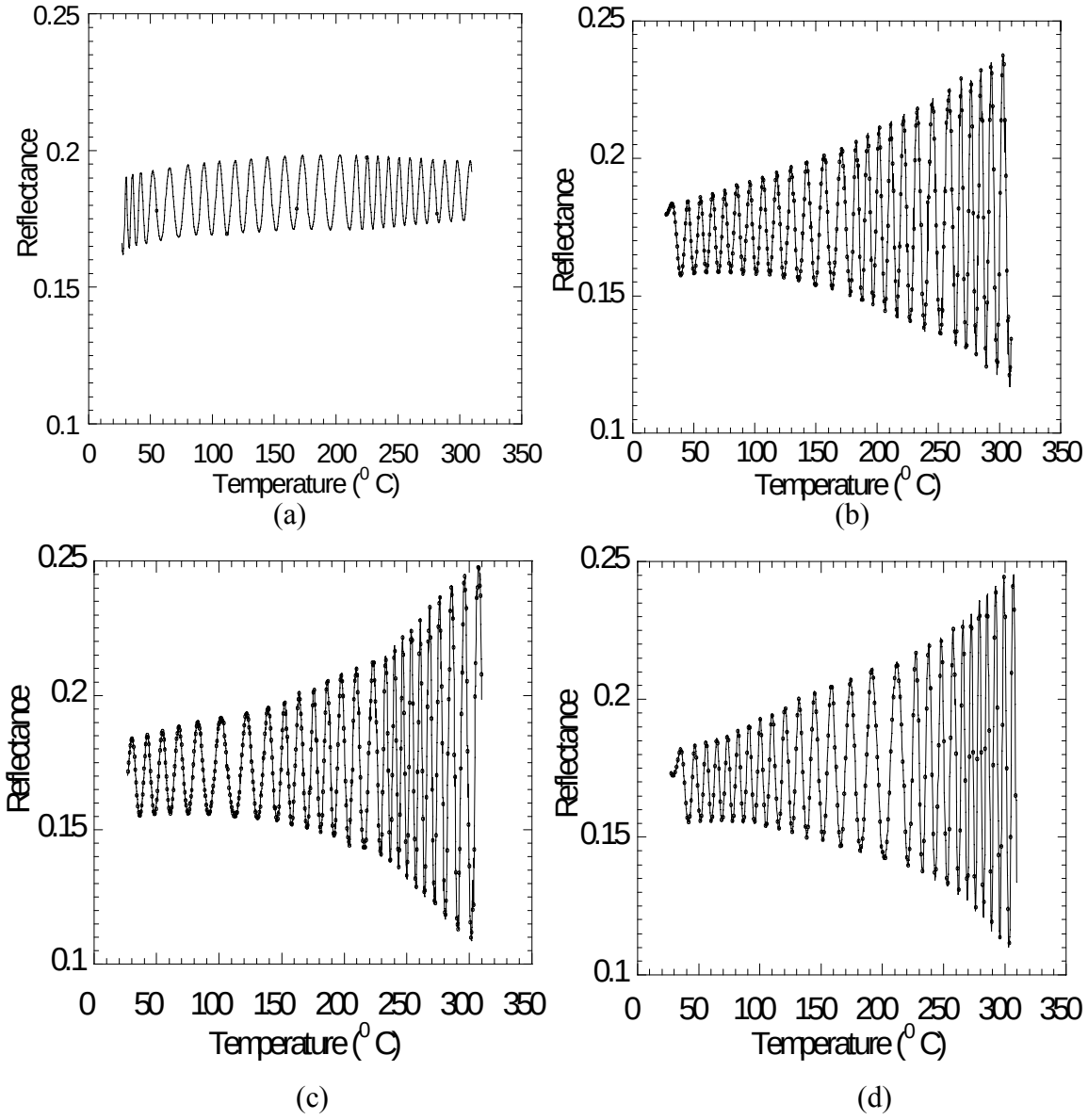

Figure 7. Optical power of Sample B SiC chip upon exposure to nitrogen gas at a pressure of (a) 14.7 psi, (b) 100 psi, (c) 200 psi, (d) 400 psi as a function of temperature from 27°C up-to 300°C for normal incidence angle (LAMMP Lab Data).

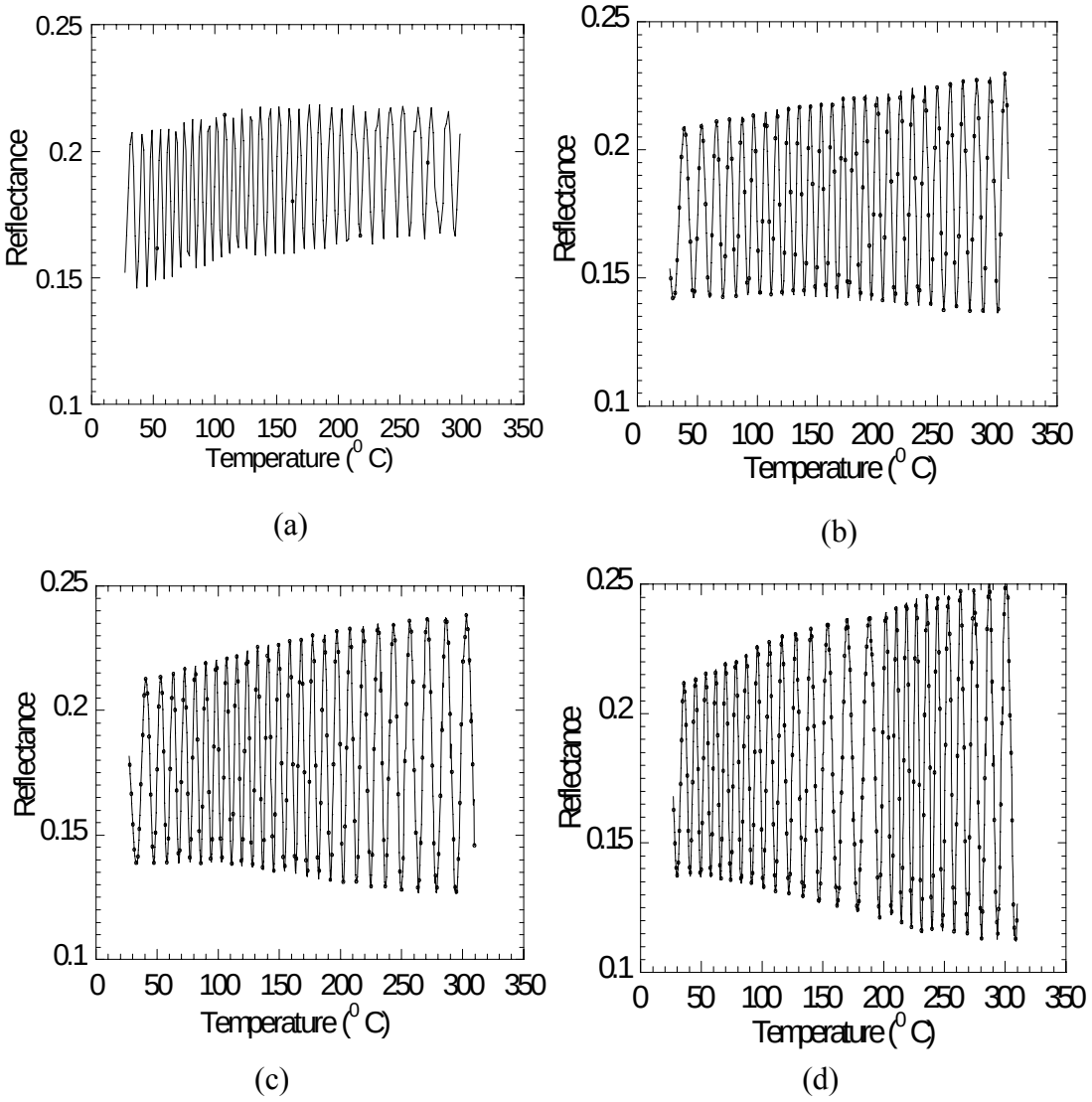

Figure 8. Optical power of Sample B SiC chip upon exposure to argon gas at a pressure of (a) 14.7 psi, (b) 100 psi, (c) 200 psi, (d) 400 psi as a function of temperature from 27°C up-to 300°C for normal incidence angle (LAMMP Lab Data).

The change in temperature at a constant pressure causes the measured optical power to oscillate between certain maximum and minimum values. These oscillations reveal an interesting pattern. Unlike the cases of atmospheric pressure [Figs. 7(a) and 8(a)], initial experimental results show the oscillations tend to diverge progressively with temperature at higher pressures. The divergence patterns of the oscillations are unique to the type of gases, i.e., nitrogen and argon in

this case, signifying that these patterns can be attributed to the characteristic identity of the individual gases in chemical sensing applications.

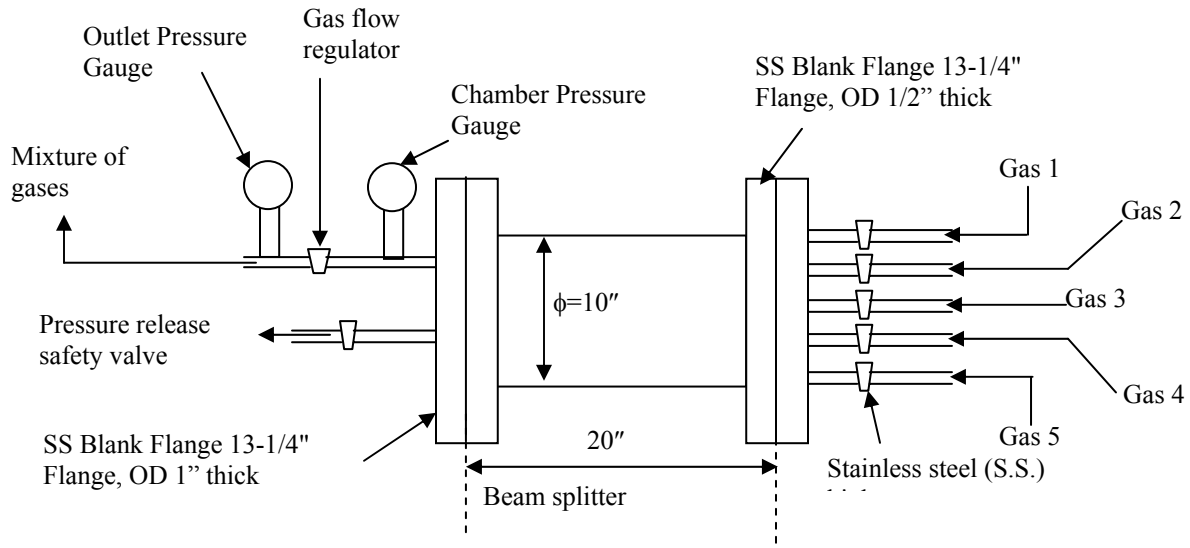

Fig.9. Schematic layout of the experimental setup used for assembling the high pressure gas mixing chamber.

Fig.9 shows the high pressure gas mixing chamber design that has been assembled in the laboratory. A purchased high pressure cylinder is used to assemble the gas mixing system. The system is built by connecting different gas ports, pressure gauges and safety valves. There are five gas ports labeled Gas 1 to Gas 5 that are connected to different gas cylinders, such as for N2, CO, CO_2, CH_4 and H_2 gases, to form gas mixtures of different partial pressures. The mixture of gases leaves the gas mixing system through an outlet on the left side of the system in Fig. 9. This high pressure gas mixture is then delivered to the SiC chip-based sensor system through an entry port in Fig. 6 so that the mixture is in contact with the chip. The chip will be heated with the induction coil in Fig.6, which, in turn, heats up the gas. Thus a high pressure and high temperature gaseous environment is created to examine the performance of the SiC gas species to be fabricated and optimized in the next phase of the project.

G.2 Sensor System for Accurate SiC Chip Thickness Measurement:

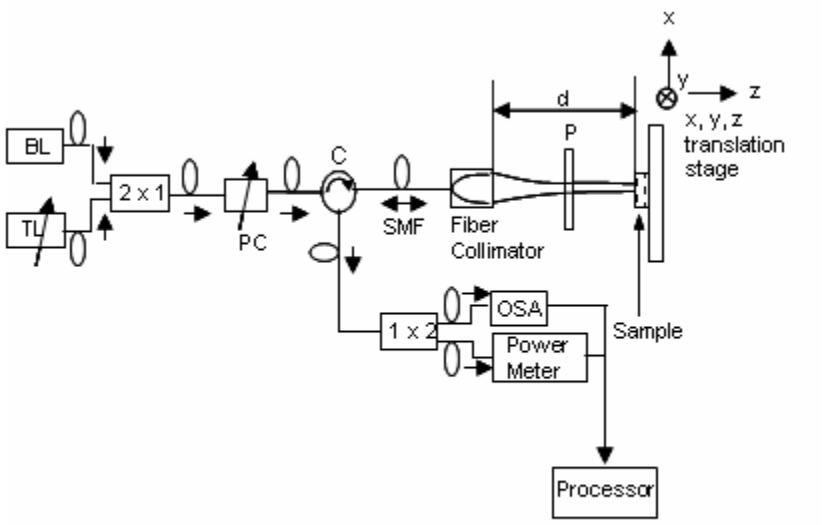

Fig.10. Proposed thickness measurement system enabling temperature probe design. BL: Broadband Light; TL: Tunable Laser; C: Circulator; P: Polarizer; PC: Polarization Controller; OSA: Optical Spectrum Analyzer; SMF: Single Mode Fiber; 2X1 / 1x2 : Fiber-Optic Switches.

Knowing the exact thickness of the sensor SiC chip is a critical need for designing the high temperature probe and also the pressure and gas sensor system. Fig.10 shows the proposed hybrid fiber-freespace thickness measurement sensor system. The Fig.10 system solves the problem of SiC chip thickness measurement by using a hybrid design that uses both fiber and free-space optics and samples such as Si and 6H-SiC whose material dispersion data via the Sellmeier equations are accurately available in the literature [6-7]. Furthermore, the typical mentioned Si and 6H-SiC substrates are thick (d >> probe wavelength λ, e.g., d=300 μm) leading to small inter-wavelength gaps (e.g., < 2 nm) that reduces thickness measurement errors due to inaccuracies in prior reported wavelength dependent refractive index data. These sample conditions are indeed met for the concerned temperature sensor applications using Si and SiC substrates.

The Fig.10 system deploys two optical processing trains. First, a moderate bandwidth (e.g., 10 nm) broadband source lights up the sample via control of a 2x1 fiber-optical switch. Light from the broadband source passes via the switch to enter a fiber-optic circulator that directs the light via a SMF to a fiber lens. This fiber lens is a special Gradient Index (GRIN) lens that

produces an output Gaussian beam with its minimum beam waist located at a distance d from the output GRIN lens surface. The location of the freespace beam waist also marks the location of the sample plane. Note that this minimum beam waist location is also where the laser beam has near perfect collimation, a condition required for high quality Fabry-Perot interferometry. Hence, plane waves are launched into the parallel faces of the sample at the localized minimum beam waist spot. To profile the entire substrate, the sample is physically translated in the plane of the beam cross-section. Thus by monitoring the received optical power, one can conclude that the sample is aligned for a thickness measurement. Because the sample refractive index and optical loss due to all system components is known, one can use Fresnel reflection coefficient theory to estimate the maximum optical power reflected from a given substrate. Hence, knowing the total expected losses from all components in the system including the test sample, one can approximate the expected optical power detected when the sample is correctly aligned. This maximized light re-coupled into the SMF passes via the circulator and another fiber-optic 1x2 switch set such that the sample reflected broadband light enters a fiber-coupled optical spectrum analyzer. The nature of the used broadband source is to provide a few observable interference fringes for the output spectrum. Hence, perhaps two to 5 fringes are needed to add a 2 to 5 redundancy into the proposed thickness measurement. Hence, unlike previous approaches that rely on extensive broadband data over continuous and very wide spectra, the proposed sensor only needs spectra data over a narrow (e.g., 10 nm) range. Specifically, the OSA is used to read the wavelength location of say 5 fringe minima positions. The accuracy of the wavelength reading depends on the resolution of the OSA, both in terms of wavelength and optical power reading. Thus, using the broadband source and OSA, a first reading of wavelength positions is noted. Next, the two optical switches in the Fig.10 system are flipped and a tunable laser and optical power meter are switched into the measurement system to take a second reading for wavelength positions. Here the tuning resolution of the laser combined with the accuracy of the power meter will determine the accuracy of the taken wavelength readings. Hence, two sets of wavelength readings can be taken to add fault-tolerance to the measurement system. Pairs of these adjacent spectral minima readings in conjunction with the pre-known sample refractive index data via the Sellmeir equations is then used to compute the sample thickness value at the given probed sample location set by the mechanical translation stage.

The optical power reflectance from a Fabry-Perot cavity is maximum for the reading of the proposed Fig.10 system are taken when the chip optical path length cosine term $cos(\phi) = 1$ or

$\phi = 2\pi m$, where m = 0,1,2,3,…., while the minimum reading of the received optical power are taken when $cos(\phi) = -1$ or $\phi = (2m-1)\pi$. Hence, as the wavelength λ of the system optical source engaging the sample changes from one spectrum minimum (or maximum) position to the adjacent mimimum position, the optical path length in the substrate has changed causing ϕ to change by 2π radians. Given that the first chosen power minimum occurs at a measured λ_1, the sample round-trip propagation phase accumulated is given by: $\phi_1 = \{4\pi\, n(\lambda_1)\, t / \lambda_1\}$. Similarly, for the adjacent power minimum occurring at a measured λ_2 value, the sample round-trip propagation phase accumulated is given by: $\phi_2 = \{4\pi\, n(\lambda_2)\, t / \lambda_2\}$. Given that for any two chosen adjacent spectra power minima with $\lambda_2 > \lambda_1$ the roundtrip optical phase changes by 2π, $\phi_1 - \phi_2$ can be written to give the sample closed-form exact optical thickness value t of:

$$t = \frac{\lambda_1 \lambda_2}{2(\lambda_2 n_1 - \lambda_1 n_2)}, \qquad (1)$$

where $n(\lambda_1) = n_1$ and $n(\lambda_2) = n_2$.

The Fig.10 system is set-up in the laboratory. The broadband source is an Edge-Emitting Light Emitting Diode (EE-LED) that acts as an internal source for the Agilent Model 86142B OSA with a direct wavelength detection resolution of 0.06 nm and an interpolated wavelength reading resolution of 0.001 nm. The tunable laser is a Santec Model TSL210 with a tuning resolution of 0.01 nm. The self-collimating fiber Graded Index (GRIN) lens from LightPath Technologies has a half self-imaging distance d of 12.5 cm. The GRIN lens forms its $1/e^2$ minimum beam waist diameter of 1 mm on the sample plane. The test substrate Si or SiC sample sits on a precision x-y-z Newport mechanical translation stage. A mechanical control Polarization Controller (PC) is used for maximizing the power in the free-space launched p-polarization of the beam. The optical circulator has a 1.7 dB optical loss. A Newport Power Meter Model 1830C and related detector Model 883IR are used for precision power measurements. By adjusting a test mirror of the x-y-z stage, the maximum free-space to SMF coupling is achieved indicating a source SMF-in to detection SMF-out total optical loss of 3.2 dB. This loss includes SMF connectors, PC, circulator, freespace-SMF coupling, and polarizer losses. Next, the SiC and Si samples are mounted on the x-y-z stage and mechanically optimized with a tilt resolution of < 0.01 degrees to

insure the equivalent low coupling loss levels. Mechanically switched fiber connectors are used instead of electronically controlled 1x2 and 2x1 optical switches to complete the data gathering. First, the OSA is used to optimize and observe the sample reflected spectrum minima wavelengths. Then the tunable laser and power meter are used to confirm these wavelength readings and optimize them if needed.

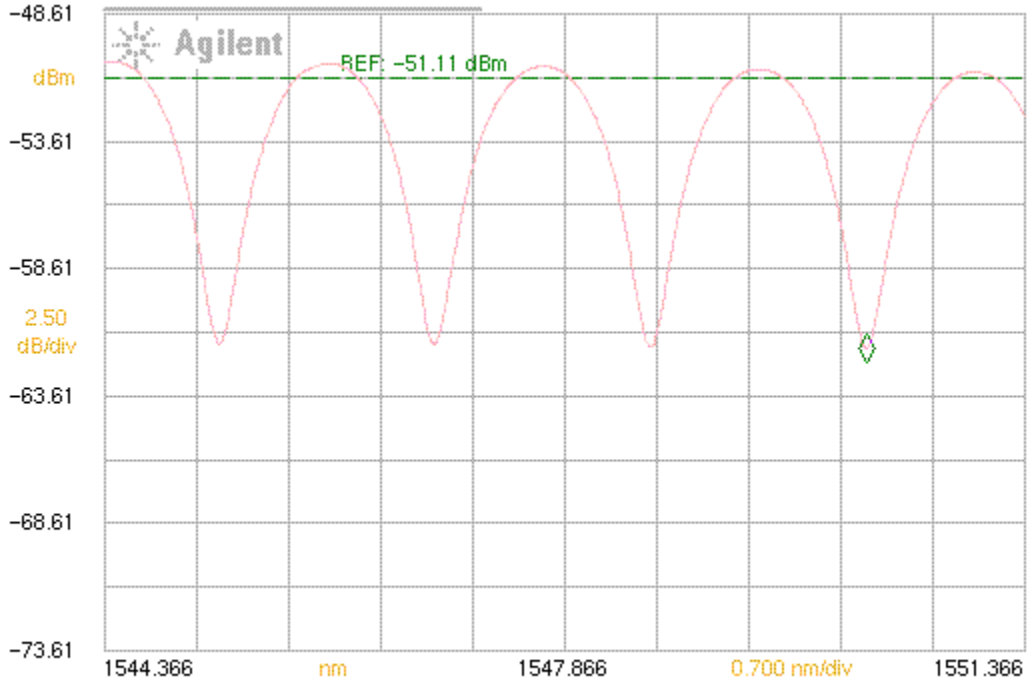

Fig. 11. OSA output for SiC sample showing the five selected wavelengths at the five consecutive optical power minima positions in the continuous spectrum.

Fig.11 and Fig.12 show the selected power minima five wavelengths for the 6-H SiC and Si substrates, respectively. In both cases, the substrate cuts are such that the material has one refractive index in the plane containing the linear polarization and these refractive indices are given by the following Sellmeier equations:

$$\text{For 6H: SiC (ordinary index);} \quad n^2(\lambda) = A + \frac{B\lambda^2}{\lambda^2 - C}, \qquad (2)$$

where A=1, B=5.5515, C=0.026406, and λ is in μm [4].

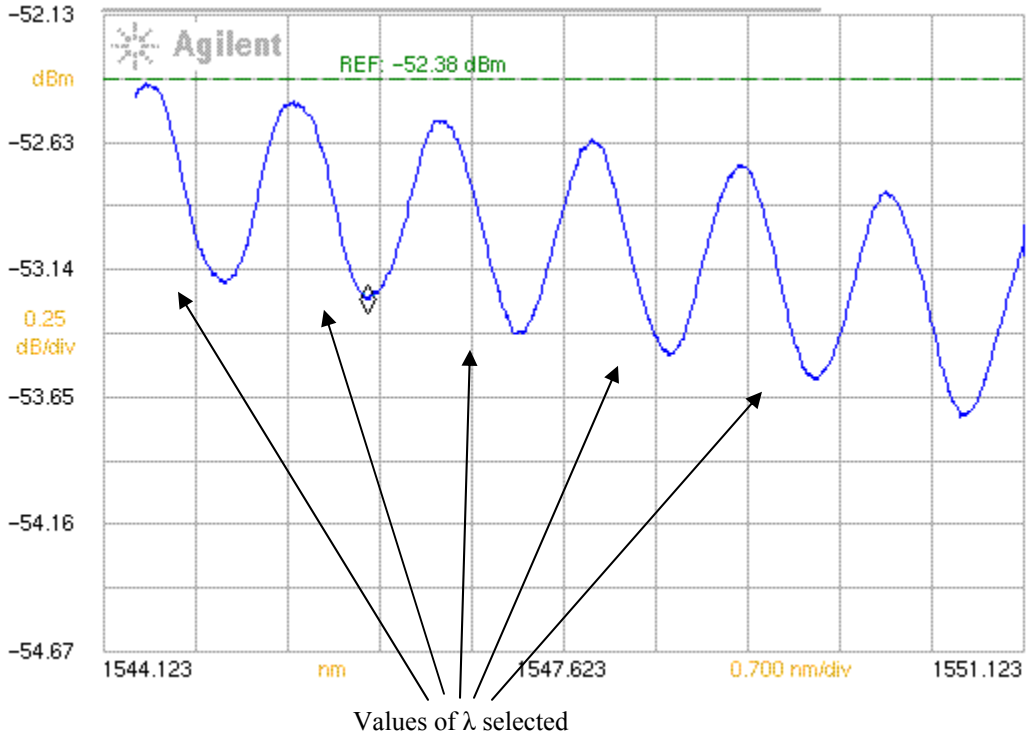

Fig. 12. OSA output for Si sample showing the five selected wavelengths at the five consecutive optical power minima positions in the continuous spectrum.

In particular, the crystal or c-axis for the given 6H- SiC chip is along the optical beam propagation direction and the crystal ordinary index is given to be normal to the crystal c-axis. Hence the incident linear polarization sees the given ordinary index in Eqn.2 for the 6H-SiC chip.

$$\text{For Si,} \quad n^2(\lambda) = \varepsilon + \frac{A}{\lambda^2} + \frac{B\lambda_1^{\,2}}{\lambda^2 - \lambda_1^{\,2}}, \qquad (3)$$

where $\lambda_1 = 1.1071$ μm, $\epsilon = 11.6858$, $A = 0.939816$, $B = 0.00810461$, and λ is in μm [3].

Table 1 shows the five measured pairs of wavelengths used for thickness processing using the relevant Sellmeier equations in Eqns 2 and 3. The wavelengths readings via the OSA has a 0.001 nm resolution. Table 1 shows the calculated refractive index values listed to the sixth decimal place, although the MATLAB program used for the thickness calculation uses numbers to the accuracy of 32 decimals places. Using the Table 1 data, the averaged experimentally measured

thickness value for the SiC sample is 281.125 μm with a ± 0.53 μm measurement accuracy. Similarly, the averaged experimentally measured thickness value for the Si sample is 296.05 μm with a ± 0.13 μm measurement accuracy.

Table 1: Experimental Results for the Calculated Thickness for SiC and Si.

	λ_1 (nm)	λ_2 (nm)	n_1	n_2	t (μm)
SiC	1551.806	1550.162	2.571585	2.571611	281.8
	1550.162	1548.517	2.571611	2.571637	281.1
	1548.517	1546.872	2.571637	2.571662	280.5
	1546.872	1545.234	2.571662	2.571688	281.1
Si	1549.539	1548.411	3.476221	3.476306	296.0
	1548.411	1547.285	3.476306	3.476391	296.1
	1547.285	1546.160	3.476391	3.476476	295.9
	1546.160	1545.038	3.476476	3.476561	296.2

SiC chip surface characterization for Temperature Probe Design:

The characterized SiC chip is shown in Fig.13. The surface profile of the chip was analyzed using the Zygo NewView 6000 series white light interferometer. The figure above shows the surface profile of a small portion measuring 1.39 mm by 1.04 mm.

A cross-section taken through Figure 13 is shown in Fig.14 and shows the characteristic surface flatness of the chip. Here the vertical axis shows the departure from flatness while the horizontal axis shows the distance along the cross-section. As can be seen from Fig.12, the surface flatness varies by only about 5 nm in the positive direction (bumps) and about 20 nm in the negative direction (valleys).

Figure 13 shows the distribution histogram of the SiC chip surface profile image. This histogram shows that 92.9% of the total pixels in the image of the chip are within ±6 nm of the mean surface flatness. As an additional sample, Fig.14 shows the surface profile taken at another location on the chip and its corresponding cross-section is shown in Fig.15.

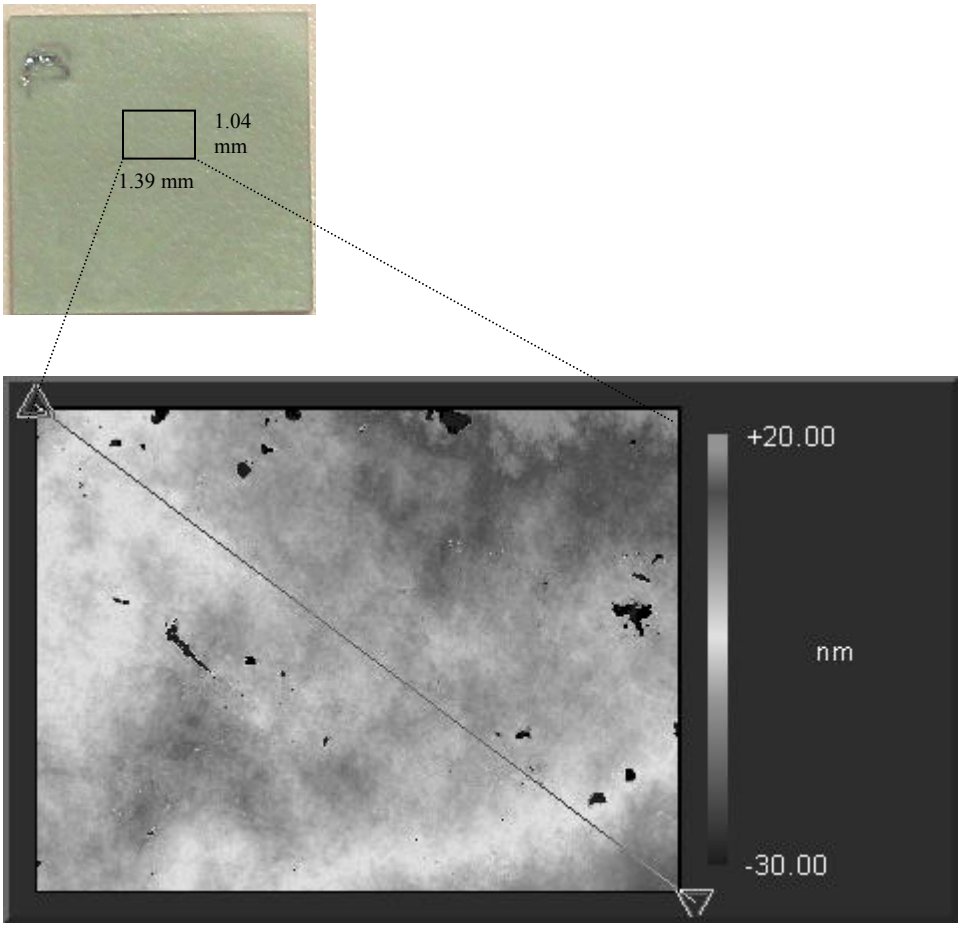

Fig.13 SiC Optical Chip top surface profile measured using a white light interferometer.

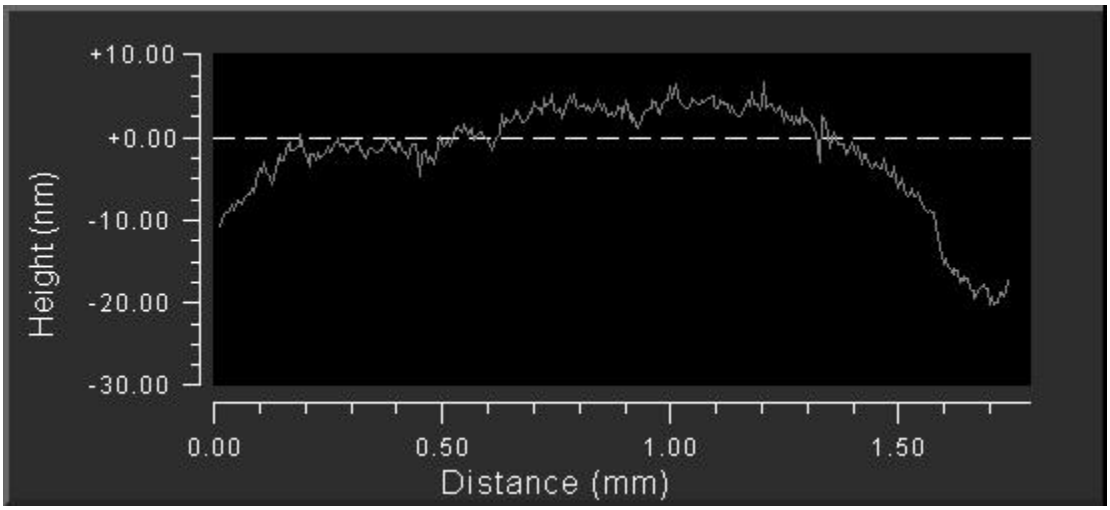

Fig.14 A cross-section taken through Figure 13 showing the characteristic surface flatness of the chip.

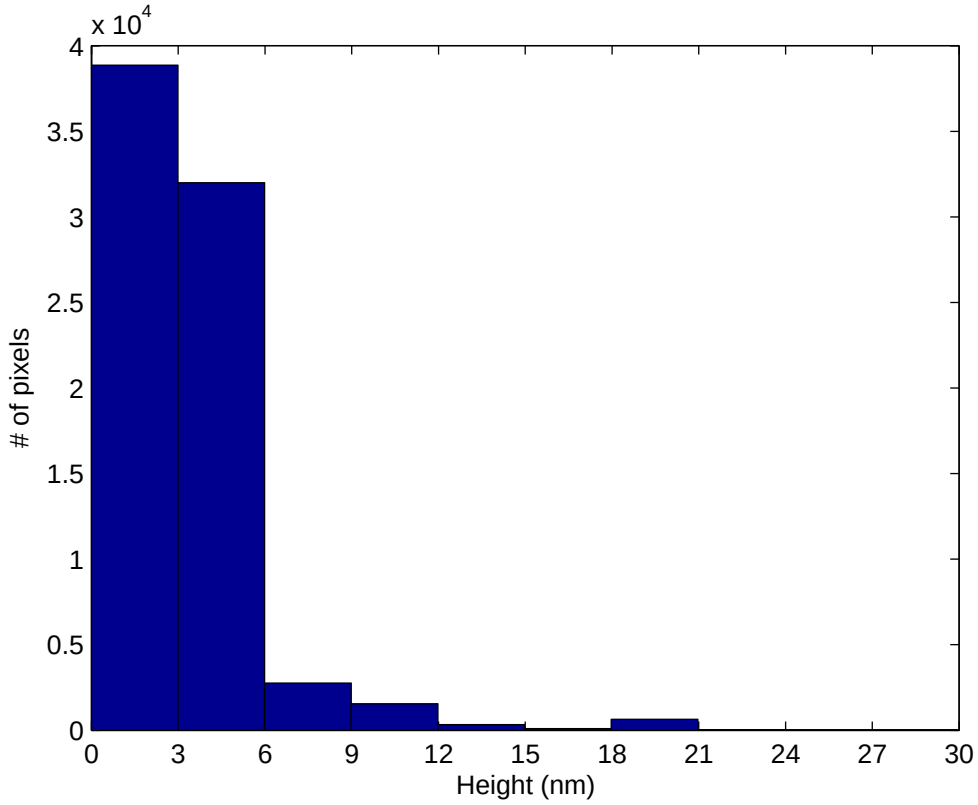

Figure 15 shows the distribution histogram of the SiC chip surface profile image.

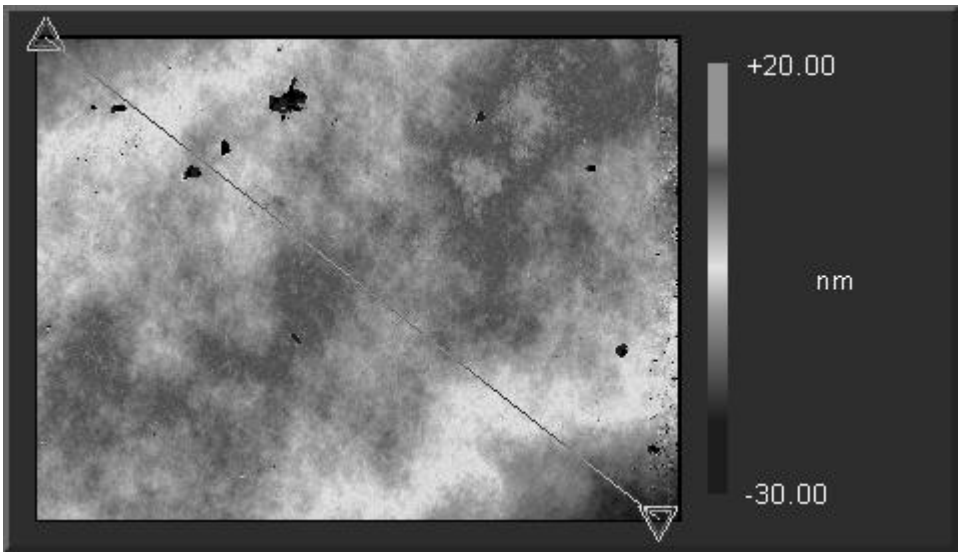

Fig.16. The surface profile taken at another location on the SiC chip and its corresponding cross-section is shown in Fig.17.

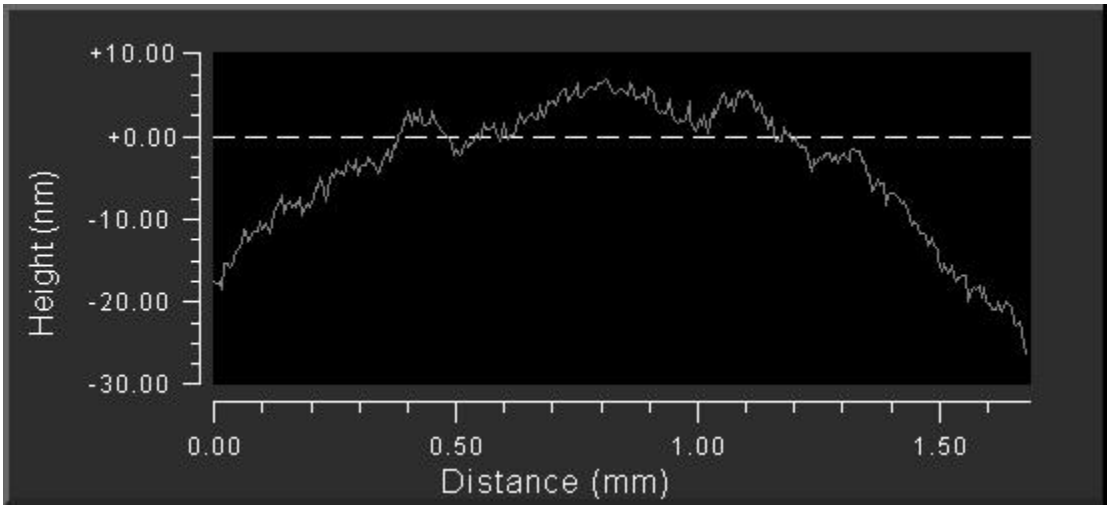

Fig.17. The surface profile cross-section taken from the Fig.16 chip image.

G.3 SiC Chip High Gas Pressure Mechanical and Optical Response Sensor System:

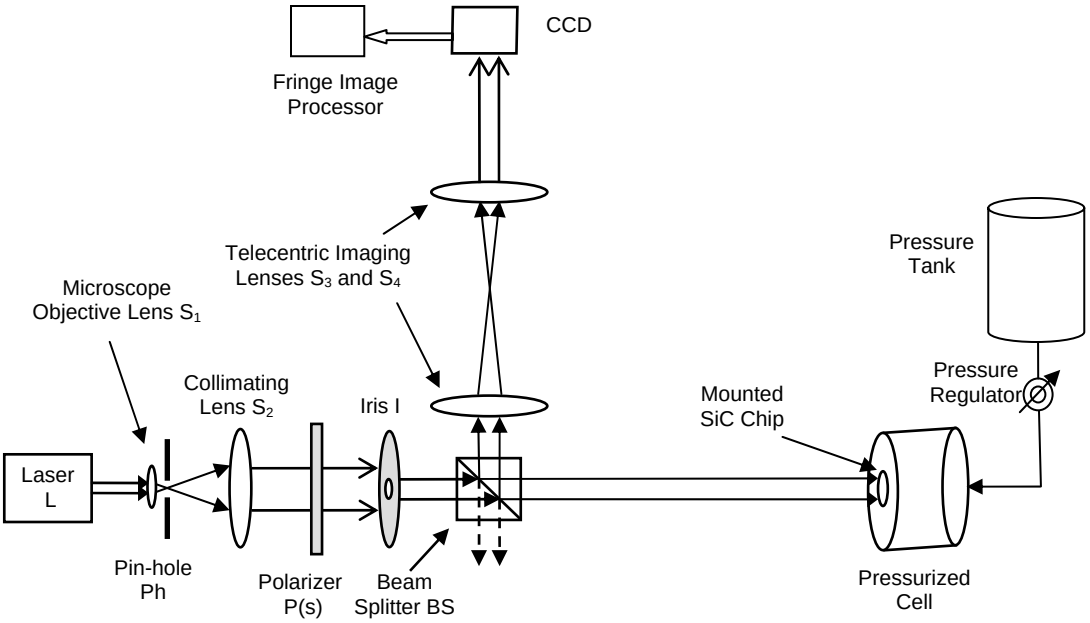

Fig.18. Proposed SiC-chip based wireless optical pressure sensor system.

The proposed SiC Chip-based optical sensor designs involve the SiC chip experiencing high pressure (e.g., 50 bar) conditions. It is critical to study the SiC chip's mechanical and optical properties under these high pressure conditions to ensure a robust performance from these SiC

chips. In order to achieve this goal, the Fig.18 proposed wireless optical pressure sensor system is set-up in the laboratory (see Fig.19 and Fig.20). The SiC chip used is the sample used in the previous section dealing with SiC chip thickness and flatness measurements.

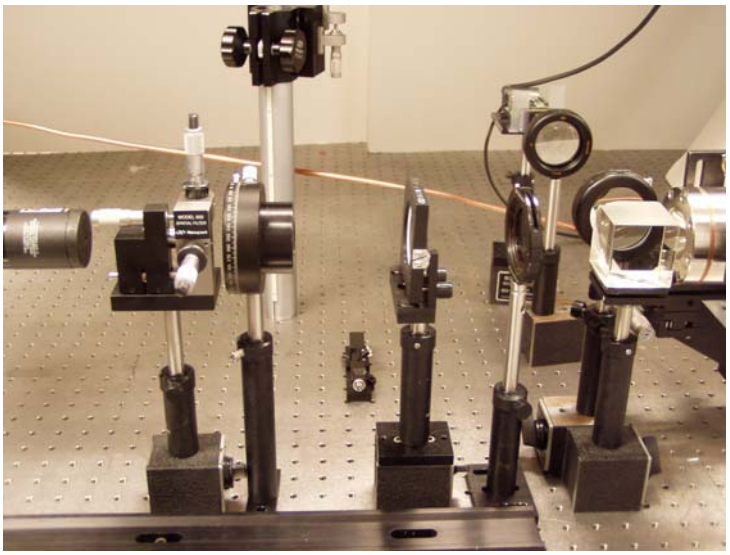

Fig.19 Experimental laboratory set-up for the SiC chip-based pressure sensor system.

Fig.20. Close-up view of the experimental SiC chip mounted in the high pressure cell.

To enable the Fig.18 experimental set-up, light from a 10 mW 633 nm HeNe laser source is passed through an expansion-filter system of 10X microscope objective lens S_1 and 10 μm pin-hole *Ph*. The cleaned and expanded beam is collimated using a 15 cm biconvex lens S_2. The beam is next vertically polarized using a polarizer *P(s)* after which it is split at the beam splitter *BS*. The portion of the light that transmits through the BS hits the SiC chip seated in the high

pressure chamber with a sealed circular boundary of ~ 5 mm diameter. The 5 mm size of the beam hitting the SiC chip is controlled by an iris *I* placed between P and the BS. Under ambient atmospheric pressure conditions (1 atm ~ 1 bar), the reflection from the front and back surfaces of the SiC chip give a phase map that represents the relative optical path length differences between the two surfaces. This phase information is seen on a 2-D CCD detector in the form of fringes.

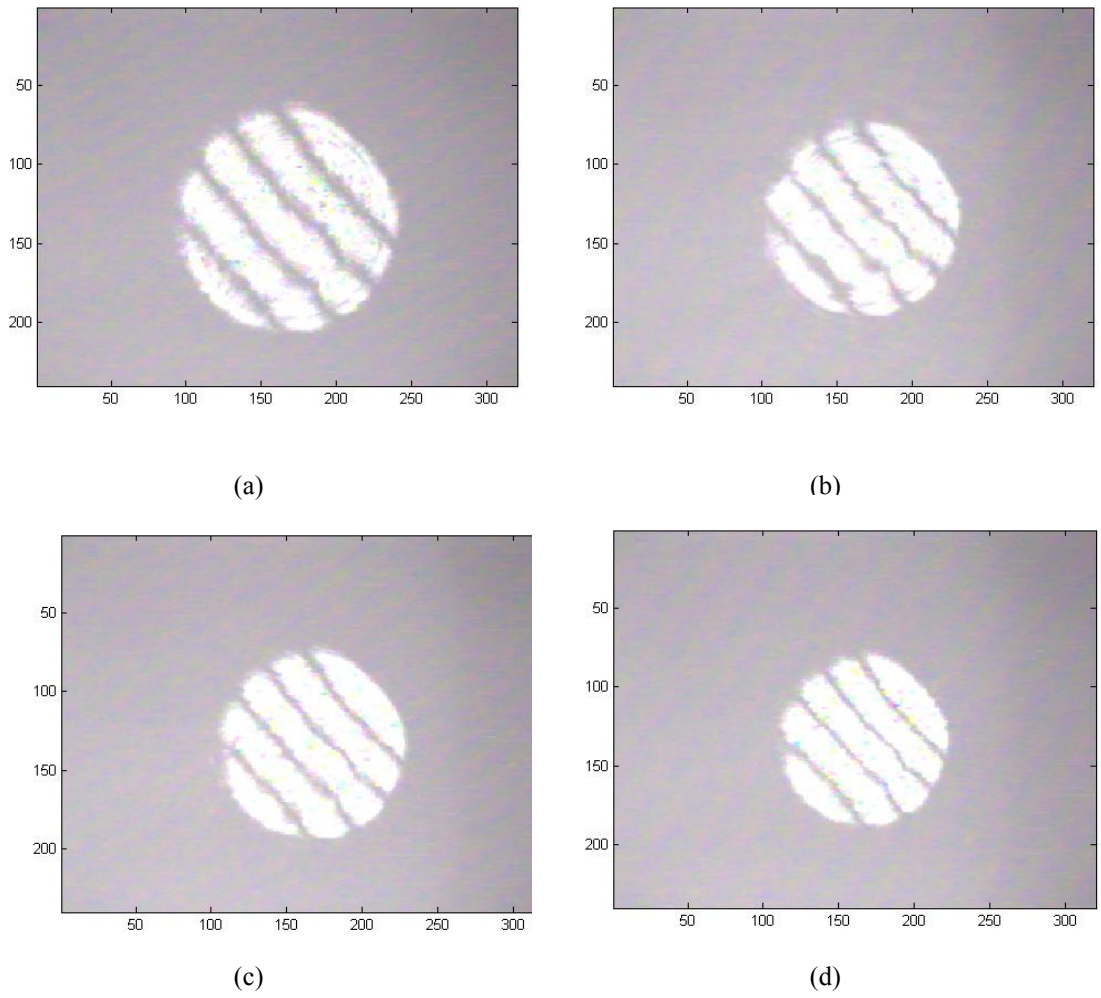

Fig.21. SiC chip-based pressure system $I_i(x,y)$ optical images produced for (a) 1 atm, (b) 13.6 atm (200 psi), (c) 27.2 atm (400 psi), and (d) 40.8 atm (600 psi) high pressure conditions.

This initial fringe pattern can be written as $I_i(x,y)$ as the initial phase map of a given SiC chip. As the pressure is increased in the high pressure cell (Fig.20), the SiC chip under small mechanical deformation conditions forms the surfaces of two convex mirrors to the incoming plane wavefronts. Given the use of the external optical imaging system in combination with the chip

mirror-like deformation, the resulting SiC chip fringe pattern $I_i(x,y)$ of a 5 mm diameter is 1:1 imaged on-to the 6.6 mm x 8.8 mm rectangular CCD plane. Depending on the pressure-based deformation of the chip, the pattern $I_i(x,y)$ undergoes reduction in size. Fig. 21 shows the set of images from the pressure sensor system where the initial fringe pattern size changes with increasing pressures up-to 40.8 atm (1 psi = 0.068 atm).

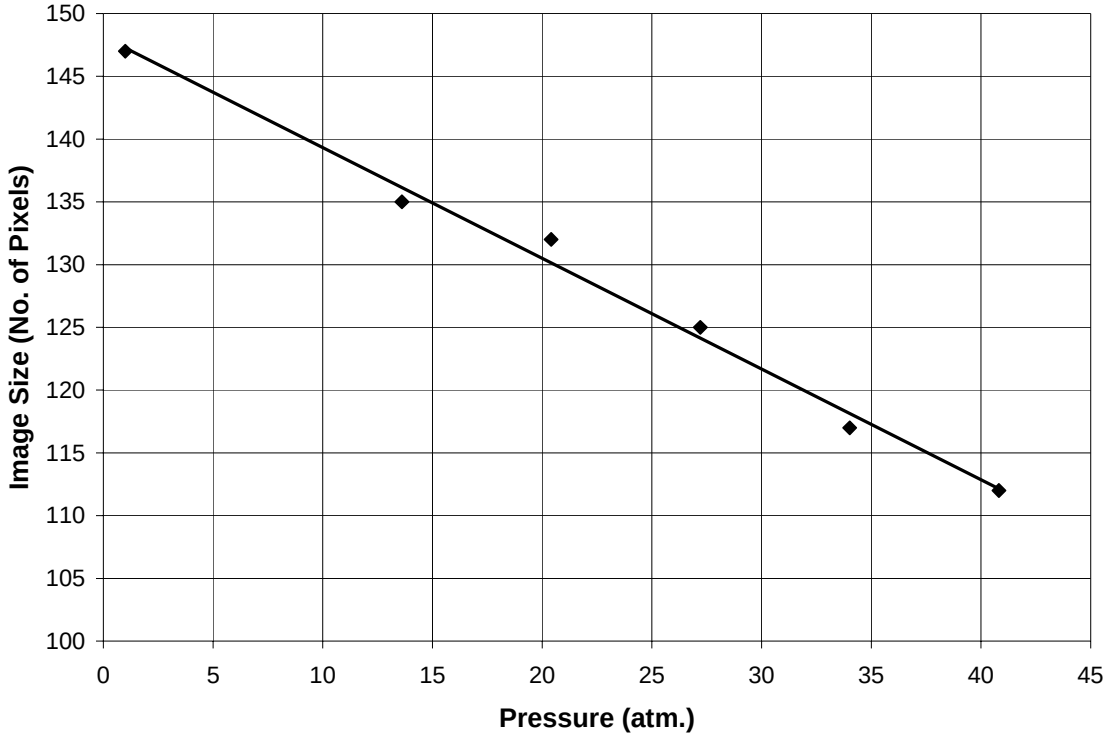

Fig.22. Optical pressure system response versus applied pressure for the SiC chip under test.

A quantization of these pressure results taken up-to 40.8 atm are represented by a pressure versus image size plot shown in Fig. 22. These results show a linear behavior of pressure versus optical parameter measurement with a current experimental resolution of 1.2 atm per image pixel (Here 147 pixels = 5 mm real size). This is to our knowledge the first demonstration of a SiC optical chip for high pressure assessment and points to the robustness of the SiC chip under high gas pressures, a result needed for proper gas species sensor system design using SiC chips.

Mechanical Response of the SiC Sensor Chip

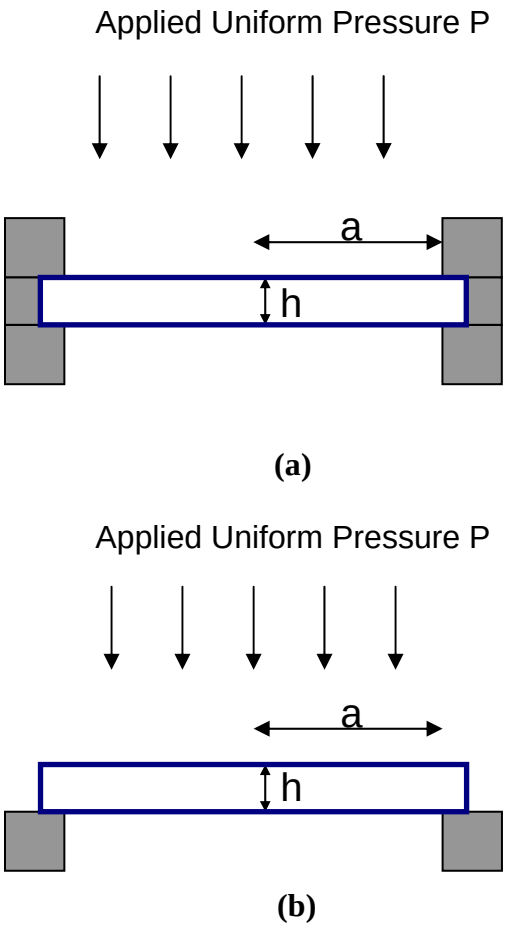

Fig. 23: Mechanical Models of SiC Sensor Chip, (a) Clamped Edge model and (b) Simply Supported model.

The mechanical response of the proposed and developed 6H-SiC chip is dependant on its mounting in the given test pressure cell. Specifically, the mounting method defines the boundary condition necessary for solving the equations that give the amount of deflection in the sensor chip. Considering the design of the given pressure cell, two major methods, namely, a circular plate/chip with 'Clamped Edges' and circular plate/chip with 'Simply Supported Edges' are analyzed for the test cell [see Fig.23(a),(b)]. In effect, the mounting method for the test cell in this study results in a hybrid-solution of the above mentioned methods. Furthermore, the deflection analysis is sub-divided under two regimes of small and large deflection analysis. The small deflection regime is defined by the condition that the maximum deflection should be less

than half the thickness of the chip [8]. The particles in the middle plane of the sensor chip undergo small displacements perpendicular to the direction of the plane thus forming the middle surface of the chip. When these displacements are small in comparison with the thickness of the chip, the strain of the middle plate can be neglected and analysis is in the small deflection regime. When this is not true, the analysis is extended to include the effect of strain of the middle plane of the chip. This large deflection regime analysis gives deflection and stress results that deviate from the small deflection regime. Finally, a failure stress analysis of the chip is essential. The maximum stress values generated for all cases have to be evaluated. Working with pressures generating maximum stress values less than the failure yield stress value for 6H-SiC ensures the reliable and repeatable performance of the sensor chip and hence the optical sensor.

Small Deflection Regime for Circular Plate/Chip with Clamped Edges

Under uniformly distributed applied pressure the circular sensor chip with clamped edges (see Figure 23(a) exhibits deflection according to the following expression [8]:

$$w(r) = \frac{P}{64D}\left(a^2 - r^2\right)^2, \tag{4}$$

where *w(r)* is the bend in chip at a certain radius *r*, *P* is applied pressure, '*a*' is the radius of the chip, 'ν' is the Poisson's ratio and *D* is rigidity constant. *D* is defined as:

$$D = \frac{Eh^3}{12(1-\nu^2)}, \tag{5}$$

where *'E'* is the modulus of elasticity and '*h*' is the thickness of the chip. The maximum deflection is at the center of the chip and is given by:

$$w_{\max} = \frac{P}{64D}a^4. \tag{6}$$

The maximum stress caused by pressure is at the boundary of the chip given by the equation:

$$\left(\sigma_r\right)_{\max} = \frac{3Pa^2}{4h^2}. \tag{7}$$

Small Deflection Regime for Circular Plate/Chip with Supported Edges

For the circular sensor chip with supported edges (see Figure 23(b)), the deflection under uniformly distributed applied pressure is given by the following expression [8]:

$$w(r) = \frac{P(a^2 - r^2)}{64D}\left(\frac{5+\nu}{1+\nu}a^2 - r^2\right). \quad (8)$$

The maximum deflection is at the center of the chip and is given by:

$$w_{\max} = \frac{Pa^4}{64D}\left(\frac{5+\nu}{1+\nu}\right). \quad (9)$$

The maximum stress in the supported chip caused by pressure is at the center of the chip given by the equation:

$$(\sigma_r)_{\max} = \frac{3Pa^2(3+\nu)}{8h^2}. \quad (10)$$

Consider the 6H-SiC chip with thickness *'h'* of 280 μm, radius *'a'* of 2.5 mm, Poisson's ratio *'ν'* of 0.16 and Young's Modulus *'E'* of 415 GPa [10].

Figure 24.a and Figure 24.b show the expected deflection and stress produced for a 6H Silicon Carbide sensor chip with applied pressure. Using a 1 GPa yield stress [10-11] (approx.) for the 6H SiC chip, the sensor chip and hence the sensor is expected to work safely up to a pressure of 100 atmospheres (atm). The maximum deflection of a 5 mm diameter pressure boundary sensor chip of thickness 280 μm is expected to be well within the small deflection range, [i.e. < Thickness/2= 140 μm], at 100 atmospheres. Comparing the two Fig.23 setups in the small deflection regime, the supported edge sensor case gives approximately 3.7~5 times larger deflection than the clamped sensor (see Fig. 24(a)) but then it also gives 1.5~1.75 times higher maximum stress value (see Fig. 24(b)). Since the experimental set-up to seat the SiC chip in the high pressure cell utilized in the study is a hybrid of the two cases, the maximum stress value is expected to be in a range whose limits are defined by the stress values given by the above two cases. Same discussion holds true for the maximum deflection of the sensor chip. Note that in the large deflection regime, exact analytical solutions are not available and only approximate analytical solutions can be utilized [9]. However, numerical methods and simulation tools (like Finite Element Method Software) can provide more exact solutions for the plate/chip deflections and stress values. Initial results indicate that the proposed and utilized SiC chip structure dimensions are robust for design in the proposed sensor systems with pressures reaching 100 atm.

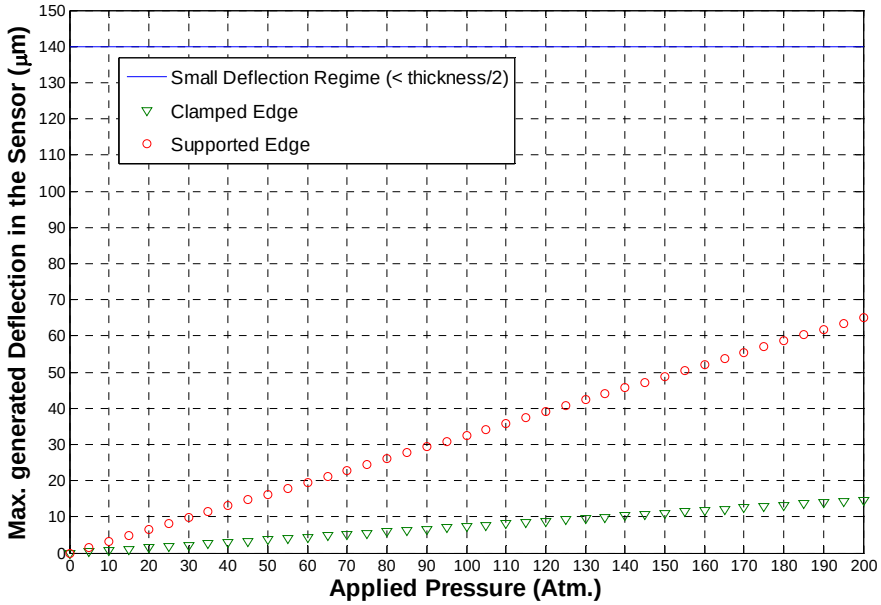

(a)

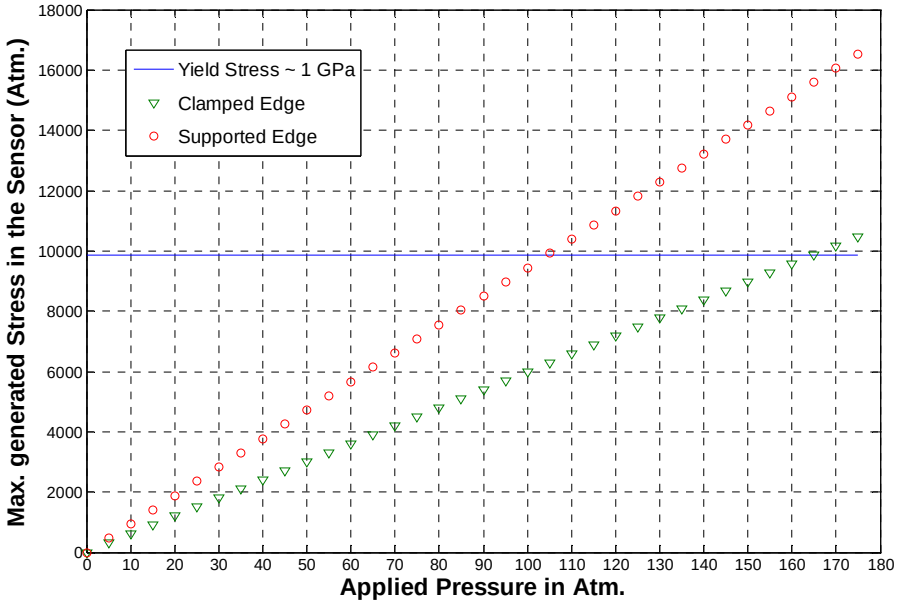

(b)

Fig. 24: The expected **(a)** deflection and **(b)** stress produced in 6H Silicon Carbide sensor chip of 5mm pressure seal diameter and 280 μm thickness.

H: RESULTS AND DISCUSSION

Gas Species SiC Chip Preparation and High Pressure Gas Mixing Chamber:

AppliCote Associates, LLC and UCF-CREOL-LAMMP (i.e., Dr. N. Quick and Dr. A. Kar) have invented a patent pending process that synthesizes embedded optical phases by a laser direct write technology **in** a substrate. The technology is an adaptation of AppliCote's patented technology to create embedded conductors in wide band-gap semiconductors. The term laser metallization is used to describe the creation of a silicon rich phase or carbon rich phase in a parent silicon carbide (SiC) substrate. Note that no metal is used. The process relies on the ability of the focused laser beam to locally change the stoichiometry of SiC through intense photonic and thermal energy coupling between the beam and substrate. These new embedded stochiometric phases exhibit refractive indexes and absorption indexes different form the parent material. To further describe the process consider a SiC wafer of top surface and a bottom surface. An incident laser beam is transmitted through the top surface and is focused by refraction within the SiC wafer to a smaller beam diameter effectively increasing the laser beam intensity. In the proof-of-concept sample described earlier and used in this study (i.e., SiC Sample A-Laser Metallized), the beam is first focused on the bottom surface and rastered upward toward the top surface (see the inset drawing in Fig.5). Hence, here there is no deterioration of the bottom surface and so the chip surface roughness is not changed form the original condition. On a status update point-of-view, a commercial prototype laser system has been designed and the appropriate laser source technology is being developed by a strategic OEM partner. AppliCote has commissioned this laser system construction with the OEM to further refine the SiC chip fabrication process. The laser system is scheduled for delivery in 3 months. AppliCote will schedule appropriate time on this system for fabricating the DOE required pertinent embedded optical devices in the up-coming 3rd year of this project. Laser doping of the SiC chips (by Kar & Quick) will also continue for optimization of chip optical response specific to individual gas species. After initial testing during fabrication phases (at AppliCote & LAMMP) and calibration studies, these chips will be incorporated by Nuonics into the proposed various sensor systems. The high pressure gas mixing chamber has also been designed and assembly in the laboratory.

SiC Chip Mechanical/Optical Surface Preparation and Temperature Probe Design:

A new SiC chip thickness measurement sensor that evolves into a temperature probe assembly has been designed and demonstrated that utilizes the intrinsic design and signal processing properties of the earlier proposed and demonstrated SiC-chip based freespace laser targeted fiber-coupled sensor. For comparison, an alternate commercial thickness measurement mechanical gauge from Mitutoyo Japan model 293-330 with a measurement accuracy with a digital readout to the nearest 1 μm (or ± 0.5 μm) is used to measure the Si and SiC sample thicknesses. Using this physical contact-based method, the thicknesses for Si and SiC samples are measured to be 296 μm and 281 μm, respectively. These comparative results are in excellent agreement with the optically measured thicknesses using the proposed system. Specifically, for the SiC case, both techniques have a near ± 0.5 μm measurement accuracy and the absolute measurements differ only by 0.125 μm or 0.044%. For the Si case, the optical measurement has a 3.8 times better measurement accuracy with the absolute thickness measurements only differing by 0.017%. In effect, the improved optical flatness quality of the optical test chip can improve the measurement accuracy from the proposed Fig.9 system.

SiC optical chip surface flatness studies have also been experimentally carried out and results indicate that the surface flatness varies by only about 5 nm in the positive direction (bumps) and about 20 nm in the negative direction (valleys). These results show that adequate wavefront quality can be obtained from today's fabricated SiC chips for use in the proposed laser-freespace target design based optical sensor systems.

The response of the SiC chip to high pressure (1 atm to 41 atm) has also been studied using a unique wireless pressure sensing system using spatial optical recognition. The initial results show a linear mechanical and optical behavior of the SiC chip with a 1.2 atm resolution indicating the robustness of the SiC chip technology under high pressures. Mechanical deflection and stress analysis indicates robust performance reaching 100 atm and beyond. These positive results attest to the strengths of SiC chip based optical sensor technology for fossil fuel based power generation system applications.

I: CONCLUSION

In conclusion, this report describes work that has evolved to meet the two quarters (6 months) stated objectives of (a) feasibility assessment of SiC chip element to detect separate simple gases through changes in refractive index with changing high temperature and high pressure and conduction of high pressure calibration studies of SiC chip and (b) assembly of a high pressure high temperature gas mixing system to produce gas mixtures and initiation of temperature probe package design. Next year starting Jan.1, 2006, we will focus on meeting objectives of fabrication via (laser) materials processing of specific embedded phase SiC chips and testing for individual gas species discrimination and implementation of temperature probe industrial requirements study.

J: REFERENCES

[1] R. Duncan, D. Gifford, V. Rajendran, " OFDR tracks temperatures on power generators," Laser Focus World Magazine, p.89, Oct. 2003.

[2] A. D. Kersey, et.al., " Fiber Grating Sensors," IEEE/OSA J. Lightwave Tech., Vol.15, No.8, pp.1442-1463, August 1997.

[3] Brian Culshaw, " Optical Fiber Sensor Technologies: Opportunities and Perhaps Pitfalls," IEEE/OSA Journal of Lightwave Technology, Vol. 22 , No. 1, pp 39 – 50, Jan. 2004.

[4] D. K. Sengupta, N. R. Quick, and A. Kar, Laser Conversion of Electrical Properties for Silicon Carbide Device Applications, *Journal of Laser Applications*, vol. 13, 2001, pp. 26-31.

[5] I. A. Salama, N. R. Quick, and A. Kar, "Laser Direct Writing and Doping of Diamond-like Carbon, Polycrystalline Diamond and Single Crystal Silicon Carbide," *Journal of Laser Applications*, Vol. 16, 2004, pp. 92-99.

[6] D.F. Edwards, "Silicon (Si)", in E.D. Palik (Ed.), *Handbook of Optical Constants of Solids*, Inc., 547 (Academic Press 1985).

[7] W. Martienssen and H. Warlimont, Eds., *Handbook of Condensed Matter and Materials Data*, XVII (Springer 2005).

[8] S. P. Timoshenko and S. Woinowsky-Krieger, Theory of Plates and Shells, Chapter 2, Pure Bending of Plates, pp. 56-57, (McGraw-Hill Inc., New York, NY 1959).

[9] S. P. Timoshenko and S. Woinowsky-Krieger, Theory of Plates and Shells, Chapter 13, Large Deflection of Plates, pp. 56-57, (McGraw-Hill Inc., New York, NY 1959).

[10] Properties of Silicon Carbide. (http://www.ioffe.ru/SVA/NSM/Semicond/SiC)

[11] Sharpe W.N., Jadaan O., Beheim G.M., Quinn G.D., Nemeth, N.N., "Fracture Strength of Silicon Carbide Microspecimens," IEEE Journal of Microelectromechanical Systems, Vol 14, No. 5, pp. 903 – 913, Oct. 2005.